Highlights:

- Presents the first physics-based control model for “PRF blended-fuel” HCCI engines.
- Provides a control model that can be utilized for real-time HCCI control.
- Validates the new model with different transient fueling experimental data.
- Illustrates the first application of Discrete Sliding Mode Control for HCCI engines.
- Provides a HCCI combustion controller with strong disturbance rejection properties.

Cycle-to-Cycle Modeling and Sliding Mode Control of Blended-Fuel HCCI Engine

M. Bidarvatan[1], M. Shahbakhti[1,*], S. A. Jazayeri[2], and C. R. Koch[3]

[1] Department of Mechanical Engineering-Engineering Mechanics, Michigan Technological University, Houghton, MI 49931, USA

[2] Department of Mechanical Engineering, K.N. Toosi University of Technology, Tehran, Iran

[3] Department of Mechanical Engineering, University of Alberta, Edmonton, Canada

[*] Corresponding author, Email address: mbidarva@mtu.edu

Abstract

Fast and robust control of combustion phasing is an important challenge for real-time model-based control of Homogenous Charge Compression Ignition (HCCI). In this paper a new discrete Control Oriented Model (COM) for predicting HCCI combustion phasing on a cycle-to-cycle basis is outlined and validated against experimental data from a single cylinder Ricardo engine. The COM has sufficient accuracy for real-time HCCI control and can be implemented in real-time.

A Discrete Sliding Mode Controller (DSMC) coupled with a Kalman filter is designed to control combustion phasing by adjusting the ratio of two Primary Reference Fuels (PRFs). The results indicate the DSMC maintains the stability of the engine operation in a wide range of loads and speeds. The DSMC is compared with an empirical Proportional Integral (PI) controller. The results show the SMC outperforms a PI controller particularly in rejecting disturbances while maintaining HCCI combustion phasing in its desired range.

Keywords: HCCI, Control Oriented Model, Model-based Control, Sliding Mode Control, Internal Combustion Engines.

1. Introduction

Optimal fuel efficiency while maintaining low emission levels are the crucial goals for powertrain manufacturers. One promising technology to reach these goals is to use Homogenous Charge Compression Ignition (HCCI). HCCI engines have high thermal efficiency, comparable to diesel engines, but have negligible particulate matter (PM) and lower nitric oxides (NO_x) emissions compared to conventional diesel and spark ignition engines (Zhao et al., 2003; Zhao, 2007). However these benefits are accompanied by major drawbacks such as limited operating range and high levels of unburned hydrocarbon (UHC) and carbon monoxide (CO) emissions (Stanglmaier, 1999; Shahbakhti et al., 2010a). Control of combustion phasing is considered the most important challenge in overcoming these drawbacks and obtaining the benefits of HCCI (Yao et al., 2004; Lu et al., 2005). Optimal combustion phasing can result in low emission levels (Koopmans et al., 2002; Xingcai et al., 2006; Shahbakhti et al., 2010a) and it influences the HCCI operating range and affects the magnitude of cyclic variations (Kalghatgi et al., 2006; Shahbakhti et al., 2008; Jungkunz et al., 2010; Shahbakhti et al., 2011). HCCI lacks a direct means to initiate combustion since it depends on charge properties such as: auto ignition characteristic, temperature, and fuel-air concentrations (Shahbakhti et al., 2007a ; Shahbakhti, 2009). The complexity of HCCI combustion control indicates that a sophisticated controller strategy which can adjust charge properties cycle-to-cycle to obtain desired combustion phasing is needed.

Different approaches and control strategies have been used in order to control HCCI combustion phasing. Fig. 1 summarizes some of the main dynamic control approaches in the literature. The HCCI controllers are divided into two main categories - empirical controllers and model-based controllers. In the first category, a manual technique is used to tune a Proportional Integral Derivative (PID) controller without incorporating a model of engine dynamics (Olsson et al.,

2001a&b; Agrell et al., 2003; Strandh et al., 2004). Model-based controllers where an accurate model is required to dynamically predict HCCI combustion phasing is the secondary category. Depending on which type of model is used in the synthesis of the controller, the model-based controllers are further subdivided into two groups: system identification-based controllers and physics-based controllers. The first group includes the controllers which are based on empirical models such as system identification or black-box modeling (Strandh et al., 2005; Bengtsson et al., 2006; Audet et al., 2009). The second group relates to model-based controllers derived from physical models such as thermodynamic models of the HCCI engine cycle. Examples of physical HCCI models are (Rausen et al., 2005; Shaver et al., 2005a & 2006; Kang et al., 2010; Shahbakhti et al. 2010b; Ma et al., 2011; Yang et al., 2011). For real-time control implementation and stability analysis (Shaver et al., 2009a), simple Control Oriented Models (COMs) have been proposed in literature (Chiang et al., 2007; Shaver et. al., 2009b; Ravi et al., 2010).

In this study, a discrete Nonlinear Control Oriented Model (NCOM) is developed for predicting HCCI combustion phasing on a cycle-to-cycle basis. The NCOM has sufficient accuracy coupled with low processing time that makes it suitable for real-time control. The crank angle where 50% of mass fraction fuel burnt ($CA50$) is used as the measure of HCCI combustion phasing. $CA50$ is used for combustion phasing since it is a robust feedback indicator of HCCI combustion phasing due to the steep heat release in the main stage of HCCI combustion (Bengtsson et al., 2006).

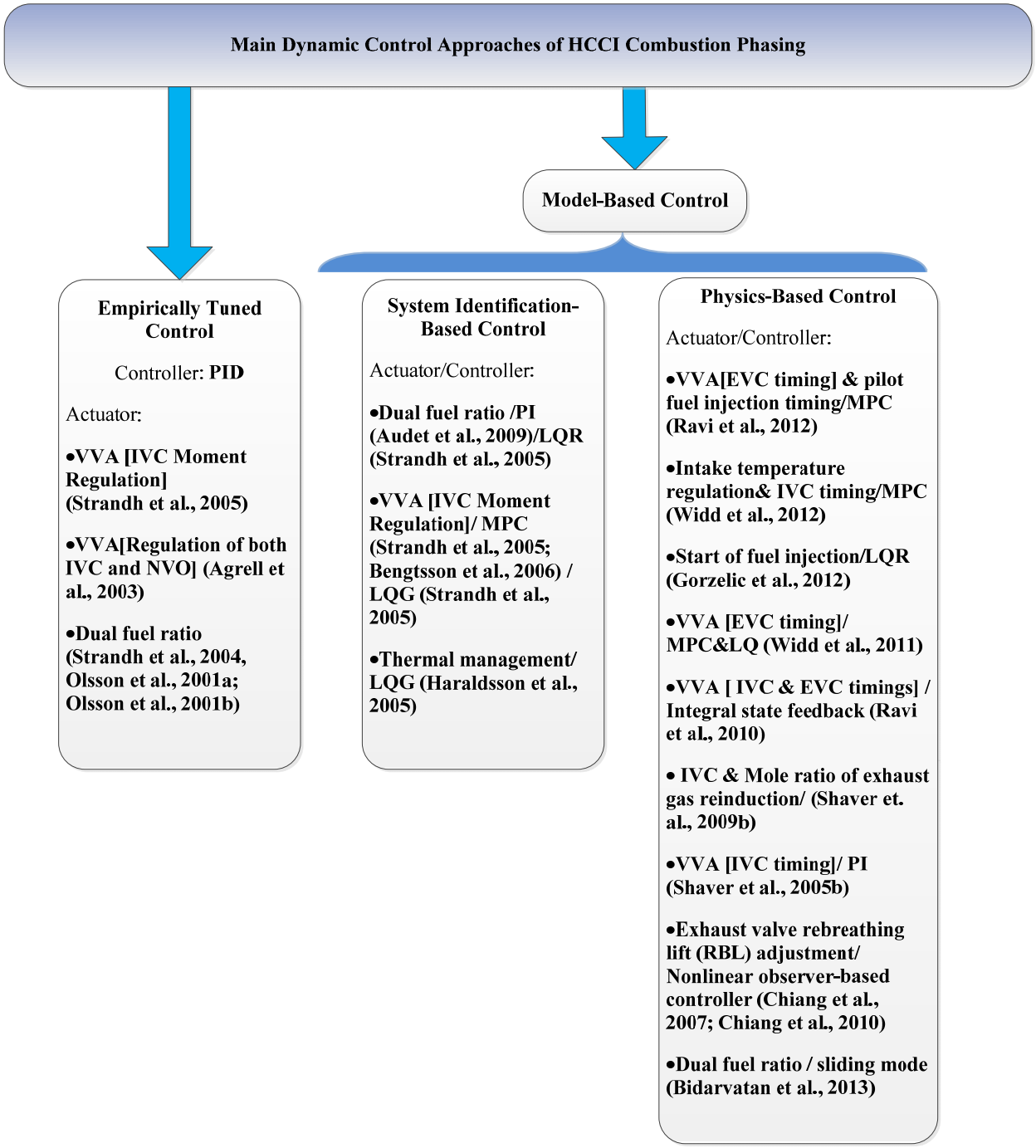

Fig. 1. HCCI combustion phasing control approaches in the literature

Fig. 1 also lists different control actuators which are used for control of HCCI combustion phasing. Examples of control actuators for HCCI include blended fuel ratio modulation (Strandh et al., 2005; Audet et al., 2009, Bidarvatan et al., 2013), charge temperature manipulation by lift adjustment of secondary exhaust valve opening (Chiang et al., 2007&2010), thermal

management (Haraldsson et al., 2005), and variable valve actuation (VVA) by intake valve closing (IVC) timing (Strandh et al., 2005; Shaver et al., 2005b; Shaver et al., 2009b), adjustment of exhaust valve closing (EVC) (Widd et al., 2011), start of fuel injection timing (Gorzelic et al., 2012), simultaneous adjustment of IVC timing and the negative valve overlap (NVO) (Agrell et al., 2003; Ravi et al., 2010), and simultaneous timing of EVC and pilot fuel injection (Ravi et al., 2012). Dual fuel control of low temperature combustion engines has recently received a lot of attention in the literature (Hanson et al., 2011; Splitter et al., 2011). This study presents dual fuel control of HCCI combustion phasing by manipulating the ratio of two Primary Reference Fuels (PRFs). This study uses a blend of iso-Octane (PRF100) with the octane number of 100 and n-Heptane (PRF0) with the octane number of 0. The reason for using a PRF fuel blend is that these fuels are standard fuels and are used to test the control to fuel octane number changes. The control strategy developed can then be suitably modified and applied to other blends of fuels.

Different types of controllers have been used in the literature to control HCCI combustion phasing. Examples of these controllers include PI control (Audet et al., 2009; Shaver et al., 2005b), integral state feedback (Ravi et al., 2010), Linear Quadratic Regulator (LQR) and Linear Quadratic Gaussian (LQG) (Strandh et al., 2005, Gorzelic et al., 2012), H_2 controller (Shaver et al., 2009b), Model Predictive Controller (MPC) (Bengtsson et al., 2006; Widd et al., 2012), and nonlinear observer based controller (Chiang et al., 2007&2010). Sliding Mode Control (SMC) is a robust non-linear control method to reject system uncertainty and disturbances. In this study, a discrete type of SMC called Discrete Suboptimal Sliding Mode Control (DSSMC) is designed for HCCI combustion phasing control. To the authors' knowledge, this is the first application of DSSMC for HCCI combustion control.

This paper is organized in sections. In the first section, a discrete NCOM is developed for HCCI combustion phasing prediction. Then, the model performance is investigated by validating it against both experimental data and simulations results from a more detailed physical HCCI model (Shahbakhti et al., 2010b). Next, a DSSMC controller along with a Kalman filter observer is designed. Tracking performance of the controller is studied under conditions of having noisy measurements and with physical disturbances. Variations in the intake manifold temperature, intake manifold pressure and the injected fuel equivalence ratio (as an engine load indicator) are considered to be physical disturbances to the HCCI engine. Finally, the control results are compared with those of a manually tuned PI controller and conclusions are reached.

2. Control Modeling

2.1. Model States and Disturbances

A discrete NCOM is developed in this section to predict cycle-to-cycle HCCI combustion phasing. The NCOM simulates an HCCI cycle by incorporating physical-empirical models to describe phenomena occurring during the HCCI cycle. The model comprises the following five states:

1- $CA50$

2- Temperature at Start Of Combustion (SOC) moment (T_{soc})

3- In-Cylinder pressure at SOC moment (P_{soc})

4- Residual gas temperature (T_{rg})

5- Mass of trapped residual gases at EVC (m_{evc})

These five states are dominant variables affecting HCCI combustion phasing since they strongly influence the thermodynamic conditions of the in-cylinder mixture in an HCCI cycle. T_{soc} and P_{soc} directly influence the location of SOC, while T_r and m_{evc} affect the charge temperature of the next cycle.

2.2. Model Description

The NCOM detailed in this section models the HCCI cycle as a series of events beginning with the intake stroke and ending with the calculation of the residual gas properties at the end of exhaust stroke. The NCOM is then parameterized for a single cylinder Ricardo engine with the specifications listed in Table 1.

Table 1 Single cylinder Ricardo engine specifications

Parameter	Value
Bore	80 mm
Stroke	88.90 mm
Compression ratio	10:1
Displacement volume	0.447 L
Number of valves	4
IVO/IVC	-175/+55 CADaBDC*
EVO/EVC	-70/-175 CADaBDC

* Crank angle degree after bottom dead center (BDC) point

The physical-empirical equations of the NCOM are described next and values of constant parameters in the NCOM are listed in Appendix A.

2.2.1. Intake Stroke (IVO ⟶ IVC)

2.2.1.1. Thermodynamic States of Fresh Charge at IVC Moment

Mixture pressure and temperature at IVC moment (P_{ivc} and T_{ivc}) are estimated by two semi-empirical correlations (Shahbakhti et al., 2010b):

$$P_{ivc,k+1} = \left[\frac{N_k^{\mathrm{a}}\, \phi_k^{\mathrm{b}}}{T_{m,k}^{\mathrm{c}}}\right] P_{m,k}\ , \tag{1}$$

$$T_{ivc,k+1} = \left(\mathrm{a}_1 T_m^2 + \mathrm{a}_2\, T_{m,k} + \mathrm{a}_3\right) \frac{\phi_k^{\mathrm{b}_1}\, N_k^{\mathrm{b}_2}}{(1+EGR)^{\mathrm{b}_3}}\ , \tag{2}$$

where EGR is the rate of external exhaust gas recirculation fraction and ranges from 0 to 1. N [rpm] is the engine speed and P_m [kPa] and T_m [°C] are the intake manifold pressure and the intake manifold temperature respectively. The index $k+1$ denotes the current engine cycle and the index k denotes the previous engine cycle.

2.2.1.2. Mixing Temperature at IVC

In-cylinder trapped residual gas from the previous cycle (cycle k) mixes with the inducted fresh charge (cycle k+1). By assuming ideal gases and energy conservation in the mixing process, the gas mixture temperature at IVC (T_{mix}) is obtained by:

$$T_{mix,k+1} = \left(1 - X_{r,k}\right) \frac{\bar{C}_{v\mathrm{nc}}}{\bar{C}_{v\mathrm{t}}}\, T_{ivc,k+1} + X_{rg,k} \frac{\bar{C}_{vrg}}{\bar{C}_{v\mathrm{t}}}\, T_{rg,k}\ , \tag{3}$$

where X_r [-] is the residual gas mass fraction. $\bar{C}_v$[kJ/kg K] is the average of gas specific heat capacity. Subscripts “t”, “nc” and “rg” denote total mixture, new charge and residual gas respectively.

2.2.2. Polytropic Compression (IVC ⟶ SOC)

By assuming a polytropic process for compression (Heywood, 1988), the instantaneous values of gas temperature and pressure are calculated between IVC and SOC as:

$$T_{soc,k+1} = T_{mix,k+1}\left(\frac{V_{ivc}}{V_{soc,k+1}}\right)^{k_c-1} , \tag{4}$$

$$P_{soc,k+1} = P_{ivc,k+1}\left(\frac{V_{ivc}}{V_{soc,k+1}}\right)^{k_c} , \tag{5}$$

where k_c is the specific heat capacity ratio in the compression process. V_{ivc} and V_{soc} are the cylinder volume at the instant of IVC and SOC. Cylinder volume at each crank angle is calculated using a slider crank mechanism equations (Heywood, 1988).

2.2.3. Combustion Period (SOC ⟶ EOC)

2.2.3.1 Combustion Phasing Prediction: MKIM Simplification

A Modified Knock Integral Model (MKIM) (Swan et al., 2007) is used to predict HCCI auto ignition phasing (θ_{soc}) (Shahbakhti et al., 2010b):

$$\int_{\theta_{ivc}}^{\theta_{soc,k+1}} \frac{\emptyset_k^{\mathrm{b}}}{A\,exp\left(\frac{\mathrm{c}\,(P_{ivc,k+1}V_c^{k_c})^{\mathrm{D}}}{T_{mix,k+1}V_c^{k_c-1}}\right)N_k} d\theta = 1 , \tag{6}$$

where θ_{ivc} is the crank angle at IVC moment. V_c and A are calculated by:

$$\mathrm{V_c} = \frac{\mathrm{V_{ivc}}}{\mathrm{V_\theta}} \qquad \mathrm{A} = \mathrm{A_1 EGR} + \mathrm{A_2} . \tag{7}$$

Although this MKIM is accurate in predicting θ_{soc}, the structure and nonlinearity limit its real-time control application to HCCI combustion phasing. Mixture temperature at IVC, fuel octane

number, and concentrations of the fuel and oxygen are the three dominant parameters influencing HCCI auto ignition phasing (θ_{soc}) (Shahbakhti et al., 2008; Chiang et al., 2006) and the fuel equivalence ratio is considered to be an indicator of the fuel and oxygen concentrations (Swan et al., 2007). The MKIM is reduced to a fitted correlation considering these three major influential parameters:

$$\theta_{soc,k+1} = f(T_{mix,k+1}, ON_k, \emptyset_k) \ . \tag{8}$$

$CA50$ is then obtained as a function of θ_{soc} and combustion duration ($\Delta\theta_{comb}$), assuming a constant fuel burn rate:

$$CA50_{k+1} = \theta_{soc,k+1} + 0.5\ \Delta\theta_{comb,k+1} \ , \tag{9}$$

resulting in:

$$CA50_{k+1} = g(T_{mix,k+1}, ON_k, \emptyset_k), \tag{10}$$

and defining the correlation as:

$$g(T_{mix,k+1}, ON_k, \emptyset_k) = \mathrm{C}_1\emptyset_k\ T_{mix,k+1} + \mathrm{C}_2\emptyset_k + \mathrm{C}_3 ON_k + \mathrm{C}_4. \tag{11}$$

The correlation given in Eq. (11) is parameterized without having external EGR and over an engine speed range of 800-1000 RPM. Values of the constant coefficients and more discussion about the correlation structure are found in Appendix A.

2.2.3.2. Thermodynamic States at EOC

The mixture temperature increase (ΔT_{comb}) assuming adiabatic combustion is determined as:

$$\Delta T_{comb,k+1} = \frac{m_{f,k+1}\ LHV_f\ \overline{CoC}}{m_{t,k+1}\ \bar{C}_v} \ , \tag{12}$$

where m_f is the mass of the inducted fuel. LHV_f is the Lower Heating Value of the blended fuel and it is a function of fuel density (ρ), volume percentage ($\%V$) and LHV of each PRF (nH denotes n-Heptane and iso stands for iso-Octane). $\overline{CoC}$ is the average completeness of combustion. The lower heating value is based on the two fuels as follows:

$$LHV_f = \frac{\%V_{nH}\rho_{nH}LHV_{nH}+\%V_{iso}\,\rho_{iso}LHV_{iso}}{\%V_{nH}\rho_{nH}+\%V_{iso}\,\rho_{iso}}. \quad (13)$$

Eq. (12) is modified to express ΔT_{comb} as a function of $\emptyset$ and X_r as:

$$\Delta T_{comb,k+1} = \frac{LHV_f\,\overline{CoC}}{(1+X_{rg,k})(\emptyset_k^{-1}\,AFR_{st}+1)\bar{C}_v}, \quad (14)$$

where AFR_{st} is the stoichiometric air-fuel ratio.

The mixture temperature at the End Of Combustion (EOC) is obtained from:

$$T_{eoc,k+1} = T_{soc,k+1} + \Delta T_{comb,k+1}. \quad (15)$$

The mixture pressure at EOC is obtained by assuming an ideal gas ($PV = m\bar{R}T$) and mass conservation during the combution period as:

$$P_{eoc,k+1} = \frac{P_{soc,k+1}\,Vsoc,k+1}{V_{eoc,k+1}}\,\frac{T_{eoc,k+1}}{T_{soc,k+1}}\,\frac{R_{eoc}}{R_{soc}}, \quad (18)$$

where R_{soc} and R_{eoc} are averages of the gas constants at SOC and EOC moments respectively. The average values are calculated for a range of ON and $\emptyset$ variations.

2.2.4. Polytropic Expansion (EOC ⟶EVO)

Expansion of burned gases after EOC is modeled as a polytropic process (Heywood, 1988) to obtain the temperature and pressure when the exhaust valve opens (EVO) as:

$$T_{evo,k+1} = T_{eoc,k+1} \left(\frac{V_{eoc,k+1}}{V_{evo}}\right)^{k_e-1}, \quad (19)$$

$$P_{evo,k+1} = P_{eoc,k+1} \left(\frac{V_{eoc,k+1}}{V_{evo}}\right)^{k_e}, \quad (20)$$

where k_e is the specific heat capacity in the expansion process.

2.2.5. Exhaust Stroke (EVO⟶ EVC)

The residual gas temperature (T_{rg}) is determined by assuming a polytropic relation for the exhaust stroke (Shaver et al., 2009b; Ravi et al., 2010; Yang et al., 2011) as:

$$T_{rg,k+1} = T_{evo,k+1} \left(\frac{V_{evo}}{V_{evc}}\right)^{k_e-1}. \quad (21)$$

The exhaust manifold pressure is considered to be at atmospheric pressure (P_0). Finally m_{evc} is obtained by applying the ideal gas state equation at Exhaust Valve Closing (EVC):

$$m_{evc,k+1} = \frac{P_0\, V_{evc}}{R_{evc}\, T_{rg,k+1}}, \quad (22)$$

where R_{evc} is the gas constant at EVC. The residual gas fraction is obtained as a mass fraction of residual gases to the entire combustion mixture and hence is calculated by:

$$X_{rg,k+1} = \frac{m_{evc,k+1}}{m_{t,k+1}}. \quad (23)$$

2.3. Model Summary

The discrete NCOM described above captures dynamics of an HCCI engine cycle as well as the thermal coupling between two consecutive engine cycles through the exhaust recirculation. The NCOM is compared with a detailed physical model simulation from previous work (Shahbakhti et al., 2010b) in Fig. 2. The complexity and nonlinearities in the NCOM are significantly reduced

from the detailed physical model. Model-based control design is easier and real time implementation of HCCI combustion phasing controller is more computationally efficient for the NCOM.

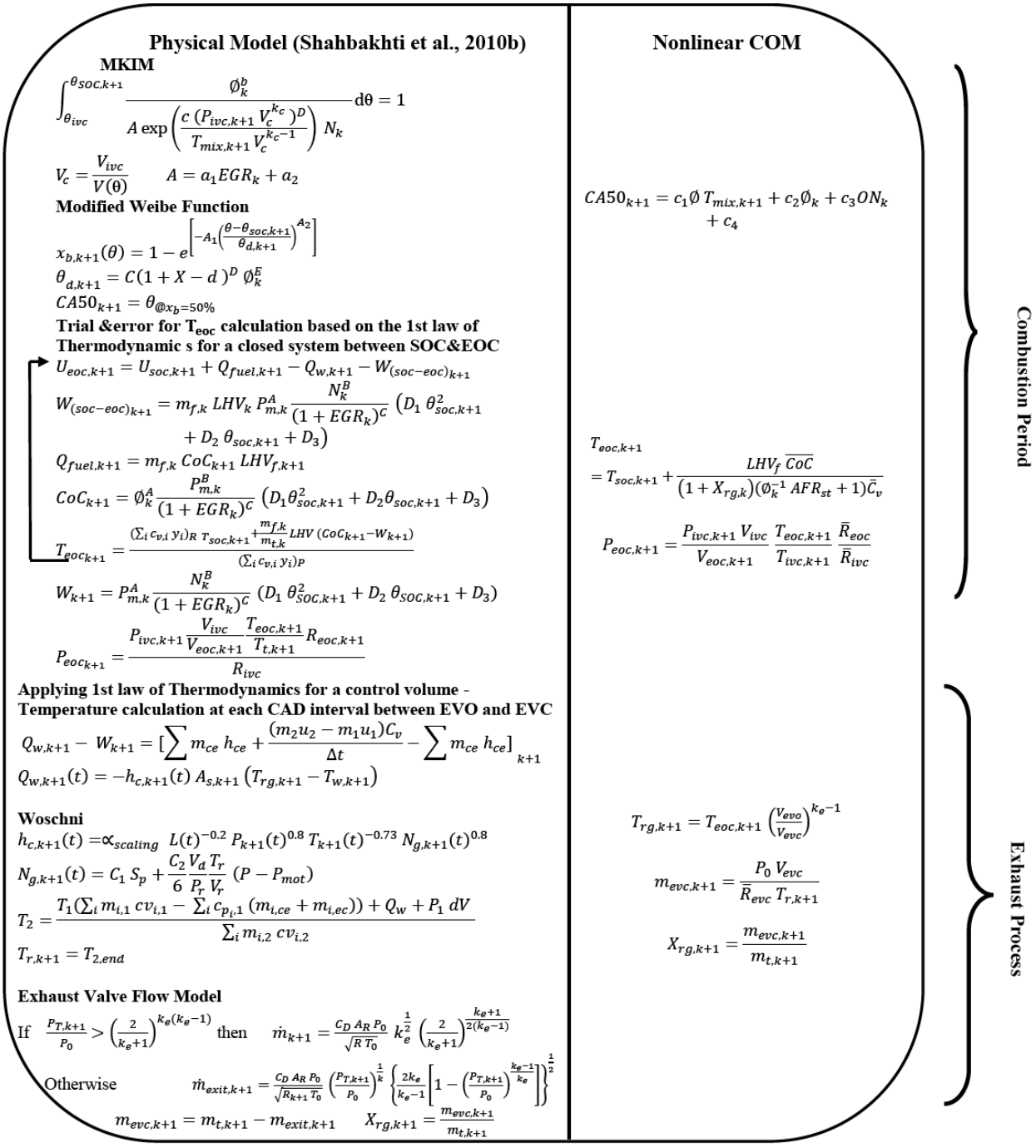

Fig. 2. Equation summary and comparison of NCOM and physical model from (Shahbakhti et al., 2010b)

Summarizing the equations in Section 2.2, the model state space and output equations are:

$$\mathbf{x_{k+1}} = F(\mathbf{x_k}, u_k), \tag{24}$$

$$y_k = G(\mathbf{x_k}), \tag{25}$$

$$\mathbf{x} = \left[CA50 \;\; T_{soc} \;\; P_{soc} \;\; T_{rg} \;\; m_{evc}\right]^T ; \; u = ON \; ; \; y = CA50, \tag{26}$$

where u is the model input, y is the output and x is the model state vector.

The NCOM and the detailed physical model (Shahbakhti et al., 2010b) are simulated for the same transient input conditions in Fig. 3. The NCOM performance is studied by comparing it to the detailed model as shown in Fig. 4. The NCOM and the detailed model show that the NCOM has good agreement for predicting the model states that are not easily measurable in practice (T_{soc}, T_{rg}, and m_{evc}). CA50 can be predicted by the NCOM with an average error and a RMSE less than 0.5 CAD.

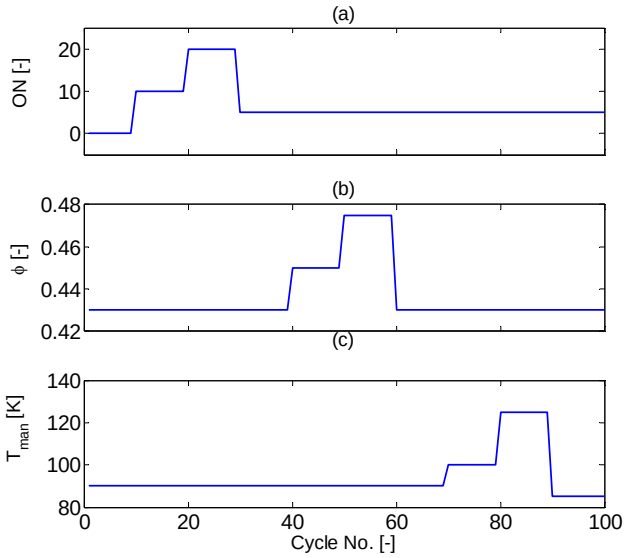

Fig. 3. Operating conditions for performance comparison test of the NCOM vs. the detailed physical model ($P_m \cong$ 110 kPa, N= 800 rpm)

The processing of 100 cycles of the physical model on a 2.67 GHz Intel processor in Fig. 4 is approximately 5 seconds. The NCOM only needs 5 ms per 100 engine cycles; a speed improvement of approximately 1000. Acceptable processing time and good accuracy in predicting $CA50$ make the NCOM suitable for real-time model-based control of HCCI combustion phasing.

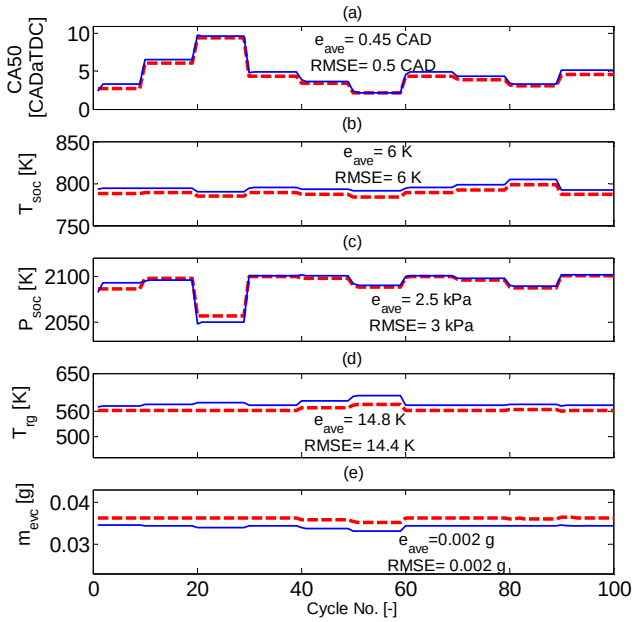

Fig. 4. Performance of the NCOM vs. the detailed physical model to predict the model states during transient engine operation shown in Fig. 3. RMSE and e_{ave} denote for root mean square error and average estimation error respectively.

3. Experimental Validation of NCOM

Before performing the control design, experimental data from the single-cylinder Ricardo engine is compared with the NCOM and the physical model to validate the models. First, both the physical model and NCOM are validated against the steady state experimental data. Experimental data at 57 steady state engine operating conditions listed in Table 2 are used to evaluate both models. The results are shown in Figure 5 and they indicate that both physical model and NCOM can capture $CA50$ with average errors of 1.3 CAD and 1.8 CAD respectively,

while the standard deviation (STD) of errors in comparison with the experimental results are less than 2 CAD for both models.

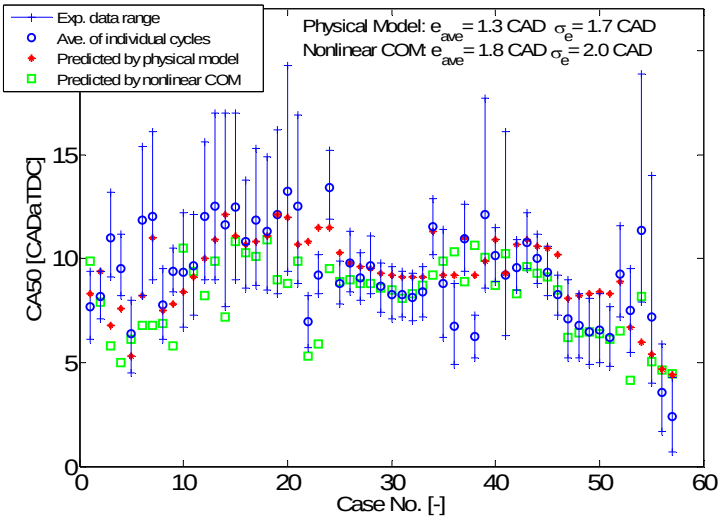

Fig. 5. Steady-state validation of the NCOM and physical model.

Table 2. Steady state engine operating conditions used for validating the NCOM.

Parameter	Value
Fuel	PRF0, PRF10, PRF20, PRF40
N [rpm]	800-1000
T_{man} [°C]	79-148
P_{man} [kPa]	89-135
$\emptyset$ [-]	0.38-0.72

Figs. 6, 7, and 8 show the performance of the NCOM and the physical model in predicting $CA50$ during transient fueling experiments. The models are tested against variations in $\emptyset$ and ON and the output $CA50$ is predicted. Results show that both models have good accuracy in predicting $CA50$ when compared to experimental engine data for the 1335 cycles tested in Figs. 6-8 with an average error and an uncertainty of error[1] of less than 1.5 CAD as well as RMSE[2] of less than 2.0

[1] Uncertainty is calculated based on standard deviation of the errors between predicted (output of the NCOM) and experimental values of CA50.

CAD. This confirms the fidelity of the NCOM for design of model based HCCI combustion timing controllers.

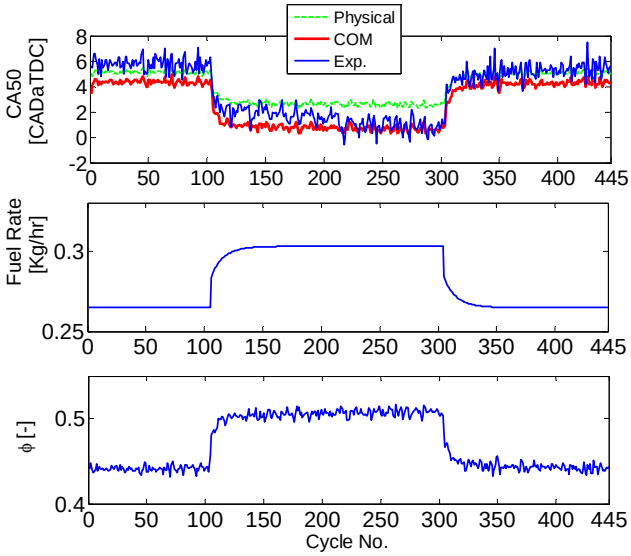

Fig. 6. One cycle ahead prediction of NCOM and physical model compared to experimental data for a fuel equivalence ratio step change (ON= 0; P_m= 100 kPa, T_m = 67 °C, External EGR= 0%, P_{exh}= 97.3 kPa, $N \cong$ 815 rpm)

[2] RMSE indicates root mean square of errors between predicted and experimental CA50s.

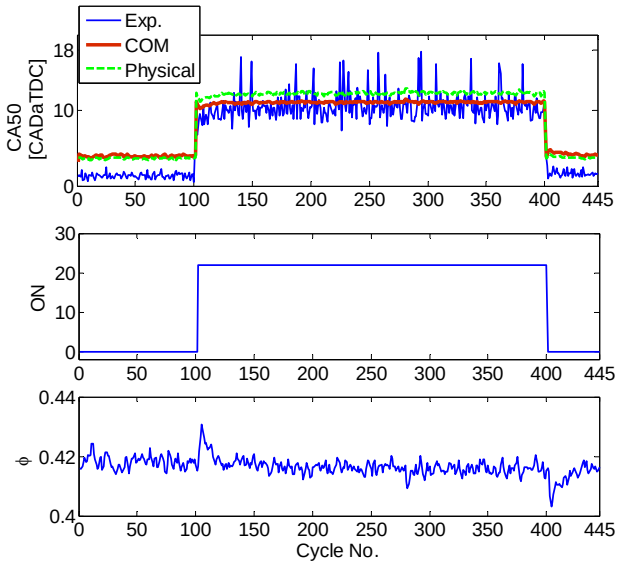

Fig. 7. One cycle ahead prediction of NCOM and physical model compared to experimental data for a fuel octane number step change (P_m= 110 kPa, T_m= 91 °C, External EGR = 0%, P_{exh}= 99 kPa, $N \cong$ 815 rpm)

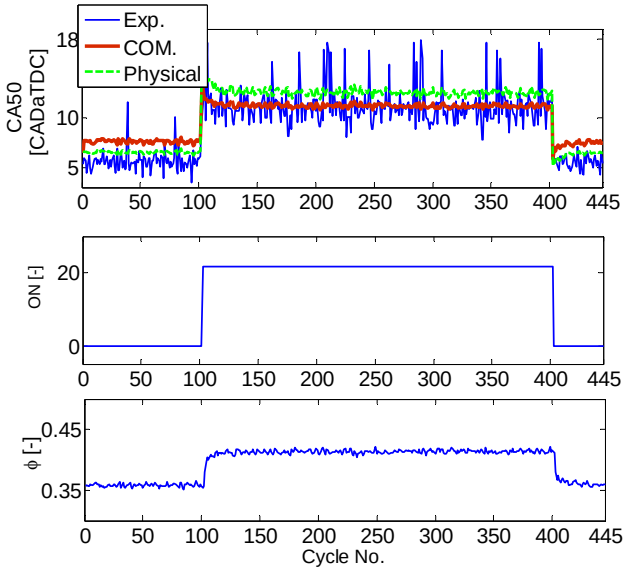

Fig. 8. One cycle ahead prediction of NCOM and physical model compared to experimental data for a simultaneous fuel equivalence ratio and octane number step changes (P_m = 110 kPa, T_m = 91 °C, External EGR = 0%, P_{exh} = 99 kPa, $N \cong$ 815 rpm)

4. Model Linearization

The NCOM is now linearized around a nominal operating point shown in Table 3. The nominal operating point is chosen using the experimental observations in (Shahbakhti et al., 2008) to ensure that the selected operating point is located in a desirable HCCI operation region. The linearized version is the following standard state space form:

$$\tilde{\mathbf{x}}_{\mathbf{k+1}} = \mathbf{A}\,\tilde{\mathbf{x}}_{\mathbf{k}} + \mathbf{B}\,\tilde{u}_k\,, \tag{27}$$

$$\tilde{y}_k = \mathbf{C}\,\tilde{\mathbf{x}}_{\mathbf{k}}\,, \tag{28}$$

where $\tilde{\mathbf{x}}$, $\tilde{y}$, and $\tilde{u}_k$ are deviations of the state vector, the output, and the input from the nominal conditions respectively.

The discrete time state space matrices **A**, **B**, and **C** of Eqs. (27) and (28) linearized about the conditions in Table 3 are:

$$\mathbf{A} = \begin{bmatrix} 0.0063 & -0.0050 & +0.0019 & -0.0226 & -116.30 \\ -0.0025 & +0.0020 & -0.0007 & +0.0090 & +46.49 \\ -0.0273 & +0.0219 & -0.0083 & +0.0990 & +507.50 \\ +0.040 & -0.0320 & +0.0121 & -0.0411 & -743.10 \\ 0 & 0 & 0 & 0 & +0.0441 \end{bmatrix}, \tag{29}$$

$$\mathbf{B} = [+0.3280 \quad -0.1311 \quad -1.4320 \quad 0.5830 \quad -0.00003]^T\,,$$

$$\mathbf{C} = [1 \quad 0 \quad 0 \quad 0 \quad 0]\,.$$

Table 3 Nominal operating point around which the NCOM is linearized

Parameter	Value
$CA50$	6 CAD aTDC
T_{soc}	795 K
P_{soc}	2104 kPa
T_{rg}	577 K
m_{evc}	0.0342 g
ON	8
$\emptyset$	0.43
T_m	90 °C
P_m	110 kPa
External EGR	0 %
N	800 rpm

At this nominal operating point the linearized system $\tilde{\mathbf{x}} = \left[\widetilde{CA50}\ \tilde{T}_{soc}\ \tilde{P}_{soc}\ \tilde{T}_{rg}\ \tilde{m}_{evc}\right]^T$ is stable. This system has five states (n=5), one input, and one output. Accuracy of the linear COM (LCOM) is tested for the experimental transient fueling conditions (Figure 9). Results show that the average error and the standard deviation of error are about 1.6 and 1.7 CAD respectively.

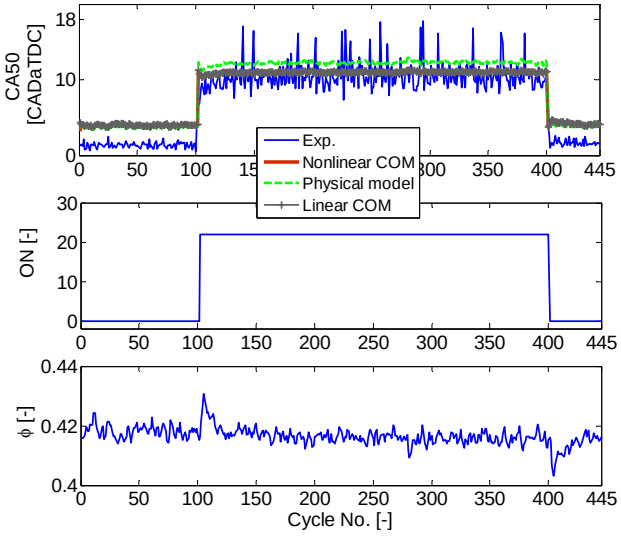

Fig. 9. One cycle ahead prediction of LCOM, NCOM, and physical model compared to experimental data for a simultaneous fuel equivalence ratio and octane number step changes (P_m = 110 kPa, T_m = 91 °C, External EGR = 0%, P_{exh} = 99 kPa, $N \cong$ 815 rpm)

5. Controller Design

5.1. Discrete-Time Sliding Mode Control (DSMC)

Discrete-time sliding mode control (DSMC), also known as quasi sliding mode control, (Milosavljević, 1985; Sira-Ramirez, 1991; Golo et al., 2000) is chosen for HCCI ignition timing control since it provides a controller design which is robust to external disturbances and uncertainties of model parameters (Bartoszewicz, 1998). Different DSMC designs are found in literature depending on what approach is used in determining sliding surface and designing switching laws. Here, a type of DSMC called discrete sub-optimal sliding mode control (DSSMC) (Yu et al., 2006) is used to control HCCI combustion phasing. In this type of controller, an optimal control law is used in determining the desirable sliding surface and the reaching phase. A Kalman filter is used to estimate the model states since most of them are difficult to measure on the engine.

5.1.1. Discrete Sub-optimal Sliding Mode Control (DSSMC) with Feed-Forward Gain

Discrete Sub-optimal Sliding Mode Control is a discrete optimization based control method that combines the advantage of optimal control with the robustness advantage of sliding mode control (Yu et al., 2006). A discrete Linear Quadratic Regulator (LQR) suboptimal control law is used for determining the sliding surface and for driving the controlled system to the determined surface. In this method, the suboptimal approach is applied to deal with backward in time calculation problem. An online-disturbance rejection rule discussed by (Su et al., 2000) is used to replace other conventional complex estimation methods (Youcef-Toumi et al., 1990; Elmali et al., 1992).

The DSSMC law is obtained by the following relation (Yu et al., 2006):

$$\tilde{u}_{DSSMC,k} = -(\mathbf{C_s B})^{-1}[\,\mathbf{C_s A}\,\tilde{\mathbf{x}}_\mathbf{k} + \mathbf{C_s B_1}\,\tilde{\mathbf{w}}_{\mathbf{k-1}}]\ , \tag{30}$$

$$\mathbf{C_s} = [\mathbf{G} \quad 1]\,\mathbf{T}\ , \tag{31}$$

$$\mathbf{T\,B} = \begin{bmatrix} \mathbf{0_{n-m\times 1}} \\ \mathbf{I_m} \end{bmatrix}. \tag{32}$$

where $\tilde{\mathbf{w}}$ is deviation of the vector of external disturbances to the controlled system from the nominal conditions, $\mathbf{C_s}$ is the sliding surface and T is an orthogonal transformation matrix that meets Eq. (32), m is a nonzero scalar, and G is calculated by:

$$\mathbf{G} = \mathbf{K} - \mathbf{S}\,. \tag{33}$$

The $\boldsymbol{K}$ matrix in Eq. (33) is obtained by LQ optimization method and matrix $\boldsymbol{S}$ is found as a function of $\boldsymbol{T}$ and a constant positive definite symmetrical matrix ($\boldsymbol{P}$) (Yu et al., 2006):

$$\mathbf{S} = -\mathbf{Q_{21}}\mathbf{Q_{22}^{-1}}\,, \tag{34}$$

where:

$$\mathbf{Q} = (\mathbf{T^{-1}})^T\mathbf{P}\,\mathbf{T^{-1}} = \begin{bmatrix} \mathbf{Q_{11}} & \mathbf{Q_{12}} \\ \mathbf{Q_{21}} & \mathbf{Q_{22}} \end{bmatrix}, \tag{35}$$

$$\mathbf{Q_{11}} \epsilon\, \Re^{n-m\times n-m}\ \ \mathbf{Q_{12}} \epsilon\, \Re^{n-m\times m}\ \mathbf{Q_{21}} \epsilon\, \Re^{m\times n-m}\ \mathbf{Q_{22}} \epsilon\, \Re^{m\times m}.$$

The first term of Eq. (30) mainly relates to regulation characteristic of DSSMC while the second term is related to robustness and its disturbance rejection property.

The main characteristic of DSSMC is robustness to external disturbances (Yu et al., 2006). These disturbances can be in terms of uncertainties in the inputs. The designed DSSMC can mitigate uncertainties in fueling amount, intake manifold temperature, and engine speed. But it cannot mitigate uncertainties in the boost pressure and mixture dilution (EGR).

A feed-forward gain ($\boldsymbol{N_u}$) is added to enhancing the controller tracking performance (Franklin et al., 1998) and the modified control law is:

$$\tilde{u}_k = -(\mathbf{C_s B})^{-1}[\,\mathbf{C_s}\,\mathbf{A}\,\tilde{\mathbf{x}}_\mathbf{k} + \mathbf{C_s B_1}\,\tilde{\mathbf{w}}_{\mathbf{k-1}}] + N_u\,\tilde{y}_r\ , \tag{36}$$

where N_x and N_u are feed-forward gain matrices used to track the reference output trajectory ($\tilde{\mathbf{y}}_\mathbf{r}$):

$$\boldsymbol{N_x}\,\tilde{y}_r = \tilde{\boldsymbol{x}}_{\boldsymbol{r}} \qquad\qquad \boldsymbol{N_u}\,\tilde{y}_r = \tilde{u}_r\ . \tag{37}$$

N_u is obtained for a system of n states (here n=5) by (Franklin et al., 1998):

$$\begin{bmatrix}\boldsymbol{N_x}\\ \boldsymbol{N_u}\end{bmatrix} = \begin{bmatrix}\mathbf{A}-\mathbf{I} & \mathbf{B}\\ \mathbf{C} & 0\end{bmatrix}^{-1}\begin{bmatrix}\mathbf{0_{n\times 1}}\\ \mathbf{I}\end{bmatrix}, \tag{38}$$

where I represents the identity matrix that is a scalar due to the unity of output.

5.1.2. Constant Gain Kalman Filter

The states of the COM ($CA50, T_{soc}, P_{soc}, T_r,$ and m_{evc}) are not easily measurable on a real engine, so a constant gain Kalman filter state observer is designed. The observed state vector ($\hat{X}$) is obtained by the following equation:

$$\hat{\mathbf{x}}_{\mathbf{k+1}} = \mathbf{A}\hat{\mathbf{x}}_\mathbf{k} + \mathbf{B}\,\tilde{u}_k + \mathbf{B_1}\tilde{\mathbf{w}}_\mathbf{k} + \mathbf{l}\,(\tilde{y}_k - \hat{y}_k)\quad . \tag{39}$$

where $\hat{y}$ is the estimated value of model output and l is the Kalman gain vector found by solving an algebraic Riccati equation by using covariance of the engine plant measurement noise (Bozic, 1979).

CA50 can be obtained by using an in-cylinder pressure sensor. If an in-cylinder pressure sensor

is used Psoc can be measured too but accurate detection of SOC can be challenging for HCCI combustion. Thus accurate measurement of Psoc is not always possible. Experimentally CA50 (Bengtsson et al., 2006) is often used.

5.1.3. Application of DSSMC for HCCI Combustion Phasing Control

Fluctuations in engine load (i.e. equivalence ratio, $\emptyset$), intake manifold temperature, and engine speed are considered as disturbances to the HCCI engine. Thus, Eq. (27) is modified to:

$$\tilde{\mathbf{x}}_{\mathbf{k+1}} = \mathbf{A}\,\tilde{\mathbf{x}}_{\mathbf{k}} + \mathbf{B}\,\tilde{u}_k + \mathbf{B_1}\tilde{\mathbf{w}}_{\mathbf{k}}\,, \tag{40}$$

where,

$$\tilde{\mathbf{w}} = \begin{bmatrix} \tilde{\emptyset} & \tilde{T}_m & \tilde{N} \end{bmatrix}^T\,, \tag{41}$$

$$\mathbf{B_1} = \begin{bmatrix} -52.980 & -0.0572 & +0.085 \\ -9.7340 & 0.4500 & 0 \\ 577.60 & 0.1140 & -0.2720 \\ 466.70 & 0.0732 & 0.0024 \\ -0.0276 & 0 & 0 \end{bmatrix}. \tag{42}$$

By applying the DSSMC from section 5.1.1 to the linearized model, the sliding surface matrix is determined for HCCI combustion phasing control:

$$\mathbf{C_s} = [-0.0268 \quad 0.0107 \quad 0.1170 \quad -0.0476 \quad -0.1501]. \tag{43}$$

The observer gain vector obtained for this engine plant is:

$$\mathbf{l} = [0.0972 \quad -0.0388 \quad -0.4243 \quad 0.1726 \quad 0]^T. \tag{44}$$

The structure of the DSSMC coupled with the Kalman filter is shown in Fig. 10.

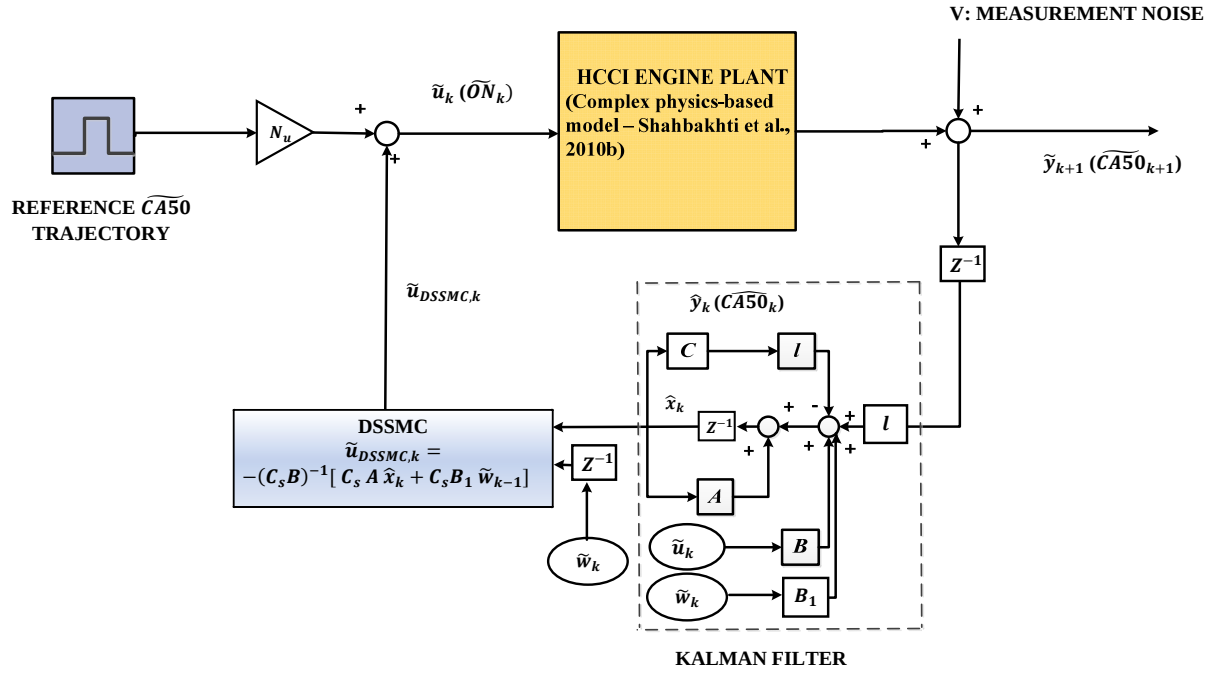

Fig. 10. Schematic of HCCI combustion phasing controller

5.2. Proportional Integral (PI) Controller

A discrete PI controller using Trapezoidal rule is designed to compare to the designed DSSMC. The discrete PI controller is:

$$G_c(z) = K_p + K_i \frac{T_s}{2}\frac{z+1}{z-1} \quad , \tag{45}$$

where K_p= 0.8 and K_i= 5.35 and T_s=150 ms. The PI controller gains (k_p and k_i) are initially set using Ziegler and Nichols method. Then both gains are varied to examine the effect on rise time and maximum overshoot. More details for selecting optimal PI gains are found in Appendix B. T_s=150 ms is the simulation sample time according to the engine speed at the nominal condition.

6. Control Results

Using the detailed physical HCCI model (Shahbakhti et al., 2010b) the DSSMC is tested. Performance of the DSSMC is then compared with the manually tuned discrete PI controller.

6.1. Tracking Performance

A comparison of tracking performance between the DSSMC and the PI controller for 100 engine cycles is shown in Fig. 11. In this figure, the octane number input is adjusted by the controller to track the desired $CA50$s while all other variables are constant. Both controllers perform well and no overshoot is observed in $CA50$ tracking results. However, the DSSMC has a 2 cycle faster rise time than the PI controller (rise times for the DSSMC and the PI controller are about 3 and 5 simulation engine cycles, respectively). Control results of DSSMC show a small steady state error (about 0.3 CAD). This is due to the model mismatch between the NCOM and the physical model.

Fig. 12 shows the observer states corresponding to Fig. 11. The accuracy of state estimation (RMSE) is also shown in Fig. 12. The RMSE values indicate the designed observer estimates the model states with a good accuracy.

Next, the performance of the DSSMC and PI controllers are evaluated for sensor noise using noisy measurements of $CA50$. The noise model assumes a Gaussian distribution with a STD of 1.5 CAD to emulate $CA50$ cyclic variations and STD_{CA50} of 1.5 CAD is chosen based on the experimental observations in (Shahbakhti et al., 2008) for the normal level of cyclic variations in the Ricardo HCCI engine. The resulting simulation is shown in Fig. 13. Under the sensor noise conditions, DSSMC has better performance with less cyclic variations as listed in Table 4. This is attributed to the observer attenuating the measurement noise.

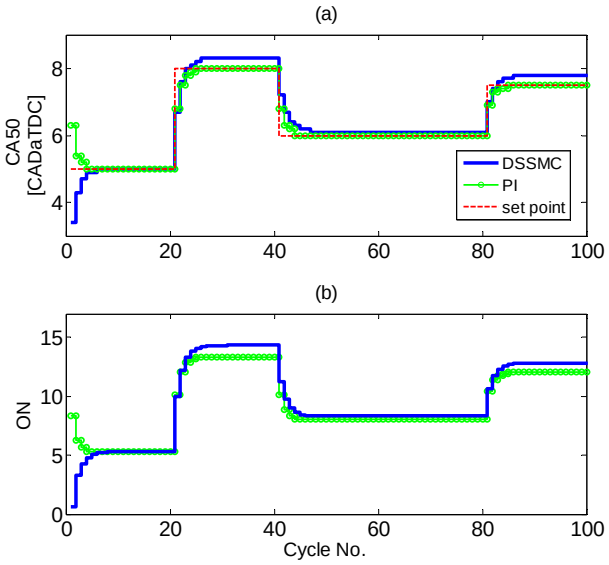

Fig. 11. DSSMC and PI controller tracking performance (a) plant (complex model) output, (b) control input

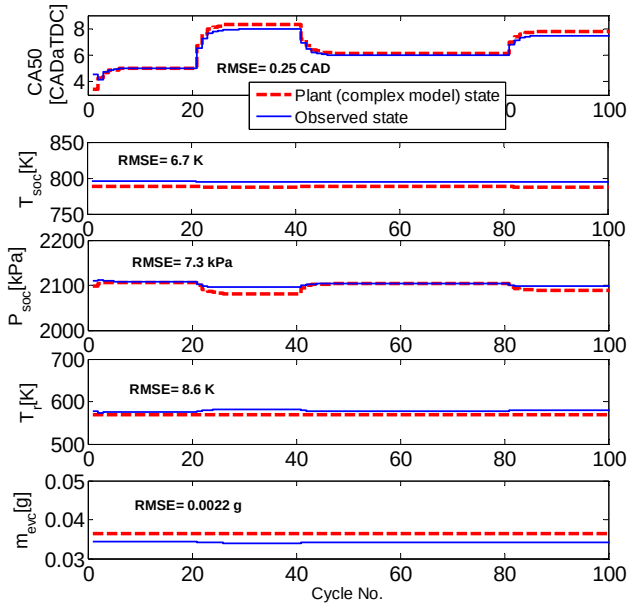

Fig. 12. State estimation of observer states corresponding to Fig. 11. RMSE is the root mean square of error values between states of the plant (complex model) and the estimated states.

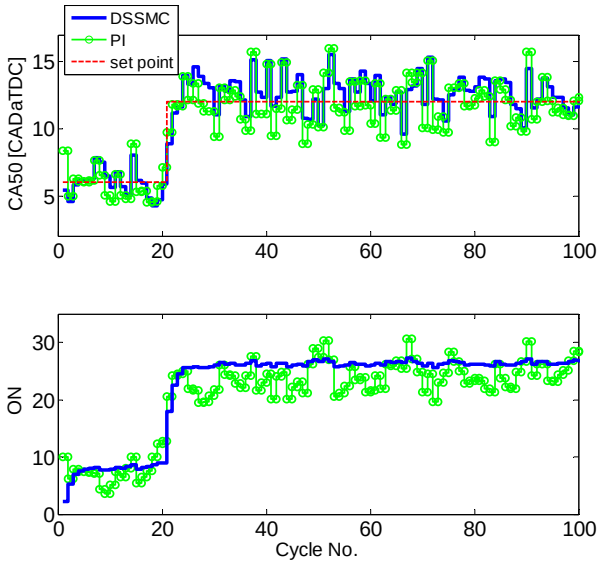

Fig. 13. Performance of controllers with measurement noise (STD_{noise} = 1.5 CAD) (a) plant (complex model) output, (b) control input

Table 4 Average cyclic errors in tracking performance of DSSMC&PI controllers in Fig. 13

Engine cycles	**STD***	
	DSSMC	**PI**
1- 20	1.01	1.30
21 - 100	1.35	1.70

*Standard deviation error of $CA50$ [CAD]

6.2. Robustness to Disturbances

A comparison for positive and negative step changes in disturbances of engine load, intake manifold temperature, and engine speed are shown in Figs. 14-16. Here the output ($CA50$ = 5 CADaTDC) is constant as the optimum set point using experimental data in (Shahbakhti et al., 2008). To judge disturbance rejection, the maximum deviation from the desired $CA50$ and the number of engine cycles each controller takes to stabilize $CA50$ to the desired steady value (within 2 %) are listed in Table 5. The DSSMC outperforms the PI controller for rejecting

disturbances. For load disturbance rejection, the DSSMC has about 3.5 CAD less average deviation to retain the desired $CA50$ compared to that of the PI controller. Similarly the DSSMC better rejects intake temperature and engine speed disturbances since it can retain the desired $CA50$ with 1.7 CAD less maximum deviation. The DSSMC has also faster response (about 3 cycles faster) in rejecting $CA50$ deviations resulted from the disturbances.

Compared to the PI controller, the model-based DSSMC is able to incorporate knowledge of the system parametric changes. Although the integral action of the PI control is mainly responsible for robustness to the physical disturbances, applying the simple on-line disturbance rejection rule (Su et al., 2000) inside the DSSMC structure enhances robustness property of this model-based controller in comparison with the PI controller. The model-based DSSMC can be utilized for other HCCI engines by parameterzing the controller model to correspond to the dynamics of a new engine.

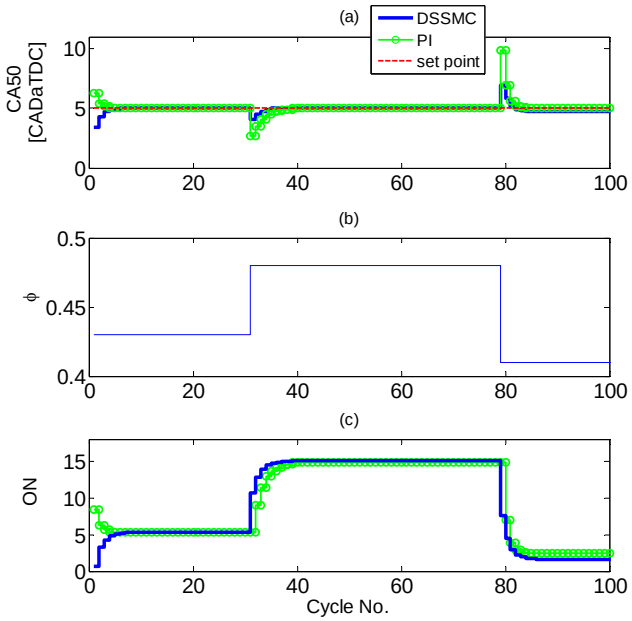

Fig. 14. Disturbance rejection: fuel equivalence ratio (engine load) step changes: 0.43-0.48-0.41 (a) plant (complex model) output, (b) disturbance, (c) control input

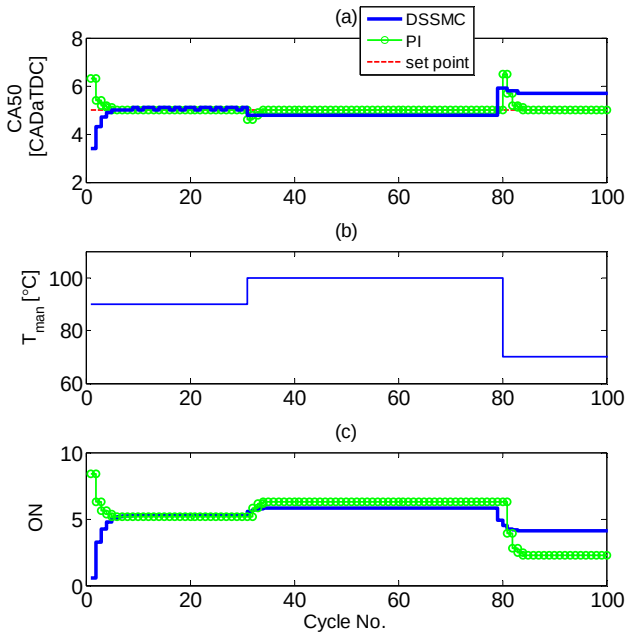

Fig. 15. Disturbance rejection: intake temperature step changes: 90 °C-100 °C -70 °C
(a) plant (complex model) output, (b) disturbance, (c) control input

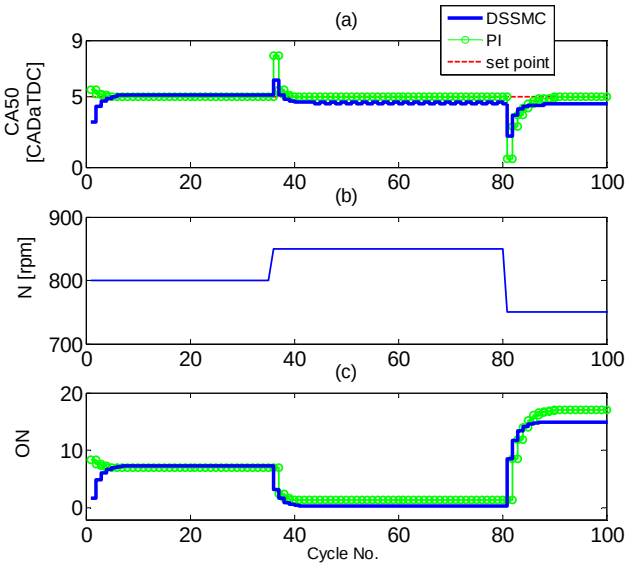

Fig. 16. Disturbance rejection: engine speed step changes: 800 rpm-850 rpm- 750 rpm
(a) plant (complex model) output, (b) disturbance, (c) control input

Table 5. Comparison of controller rejection to the physical disturbances in Figs. 14-16

Disturbance	Controller	Max. Deviation [CAD]	Rejection Speed* [cycle]
$\emptyset$	PI	5.0	7
	DSSMC	1.8	4
T_m	PI	1.5	5
	DSSMC	1.0	4
N	PI	4.5	6
	DSSMC	2.8	3

* Number of simulation engine cycles for rejecting the physical disturbances within 2 %

7. Summary and Conclusions

A NCOM is developed for predicting cycle-to-cycle HCCI combustion phasing. The NCOM is based on relations directly linked to thermodynamics of a blended-fuel HCCI engine cycle. First the model is validated against a detailed physical model and then is validated for transient operating conditions using experimental measurements. Sufficient accuracy in predicting HCCI combustion phasing and high computational efficiency make this model suitable for real-time engine control. Model processing time for one engine cycle on a 2.67 GHz Intel processor is less than 1 ms.

The NCOM is used to design a model-based HCCI combustion controller by linearization around a nominal operating point. The point is chosen using our previous experimental observations in (Shahbakhti et al., 2008) to ensure that it is located in a desirable HCCI operation region. A discrete sub-optimal sliding mode controller along with feed-forward gain is designed to control HCCI combustion phasing ($CA50$) in a range of operating conditions. The controller adjusts the injected ratio of two fuels to change octane number and obtain a desired $CA50$. Performance of the controller is compared using a detailed physical model. Simulation results show the designed controller regulates $CA50$ within a maximum of three engine cycles with no overshoot or chattering. Subject to step disturbances, the designed controller outperforms a PI controller for

rejecting step disturbances of engine load, intake temperature, and engine speed and appears promising for real-time HCCI combustion timing control.

References

Agrell, F., Ångström, H.E., Eriksson, B., Wikander, J. & Linderyd, J. (2003). Integrated simulation and engine test of closed-loop HCCI control by aid of variable valve timings. *SAE Transactions*, 112(3), 1078-1091.

Audet, A. & Koch, C. R. (2009). Actuator comparison for closed loop control of HCCI combustion timing. *SAE paper 2009-01-1135*.

Bartoszewicz, A. (1998). Discrete-time quasi-sliding mode control strategies. *IEEE Transactions on Industrial Electronics*, 45(4), 633–637.

Bengtsson, J., Strandh, P., Johansson, R., Tunestål, P. & Johansson, B. (2006). Hybrid control of homogeneous charge compression ignition (HCCI) engine dynamics. *International Journal of Control*, 79(5), 422–448.

Bidarvatan, M., Shahbakhti, M. (2013). Two-Input Two-Output Control of Blended Fuel HCCI Engines. *SAE paper 2013-01-1663*.

Bozic, S. M. (Svetozar Mile). (1979). Digital and Kalman filtering : an introduction to discrete-time filtering and optimum linear estimation. *Edward Arnold*. London.

Chiang, C. - J. & Stefanopoulou, A. G. (2006). Sensitivity analysis of combustion timing and duration of Homogeneous Charge Compression Ignition (HCCI) Engines. *Proceeding of the 2006 American Control Conference*, June 2006, Minneapolis, Minnesota.

Chiang, C.-J. , Stefanopoulou, A. G. & Jankovic, M. (2007). Nonlinear observer-based control of load transitions in homogeneous charge compression ignition engines. *IEEE Transactions on Control Systems Technology*, 15(3), 438–448.

Chiang, C.-J., Huang, C.-C. & Jankovic, M. (2010). Discrete-time cross-term forwarding design of robust controllers for HCCI engines. *2010 American Control Conference*, 2218-2223, June 30-July 2, Baltimore, MD.

Elmali, H. and Olgac, N., (1992). Sliding Mode Control with Perturbation Estimation (SMCPE): A New Approace. *International Journal of Control*, 56, 923-941.

Franklin, G. F., Powell, J.D. & Workman, M. L. (1998). *Digital Control of Dynamic Systems*. (2nd ed.). Addison Wesley.

Gorzelic, P., Hellström, E., Stefanopoulou, A. G. & Jiang, L. (2012). Model-based feedback control for an automated transfer out of SI operation during SI to HCCI transitions in gasoline engines. *5th Annual Dynamic Systems and Control Conference*, Fort Lauderdale, FL, USA, Accepted for publication.

Golo, G. & Milosavljević, C. (2000). Robust discrete-time chattering free sliding mode control. *Systems & Control Letters*, 41(1), 19–28.

Haraldsson, G., Tunestål, P. & Johansson, B. (2005). Transient control of a multi cylinder HCCI engine during a drive cycle. *SAE paper 2005-01-0153*.

Heywood, J. B. (1988). *Internal combustion engine fundamentals*. New York: McGraw-Hill.

Jungkunz, A. F. , Liao, H-H., Ravi, N., Gerdes, J. C. (2010). Reducing combustion variation of late-phasing HCCI with cycle-to-cycle exhaust valve timing control. *6th IFAC Symposium Advances in Automotive Control*, 815-820, July 2010, Schwabing, Munich.

Kalghatgi, G. T. & Head, R. A. (2006). Combustion limits and efficiency in a Homogeneous charge compression ignition engine. *International Journal of Engine Research.* 7(3), 215–236.

Kang, J.-M., Druzhinina, M. (2010). HCCI engine control strategy with external EGR. *2010 American Control Conference*, 3783-3790, June 30-July 2, Baltimore, MD.

Kirchen, P., Shahbakhti, M. & Koch, C. R. (2007). A skeletal kinetic mechanism for PRF combustion in HCCI engines. *Journal of Combustion Science and Technology*, 179(6), 1059-1083.

Koopmans, L., Backlund, O. & Denbratt, I. (2002). Cycle to cycle variations: their influence on cycle resolved gas temperature and unburned hydrocarbons from a camless gasoline compression ignition engine, *SAE paper 2002-01-0110*.

Lu, X., Chen, W., Hou, Y. & Huang, Z. (2005). Study on the ignition, combustion and emissions of HCCI combustion engines fueled with primary reference fuels. *SAE paper 2005-01-0155*.

Ma, H., Xu, H.-M. & Wang, J.-H. (2011). Real-time control oriented HCCI engine cycle-to-cycle dynamic modeling. *International Journal of Automation and Computing*, 8(3), 317-325.

Milosavljević, C. (1985). General conditions for the existence of a quasi-sliding mode on the switching hyperplane in discrete variable structure systems. *Automation and Remote Control*, 46, 307-314.

Olsson, J.O., Tunestål, P. & Johansson, B. (2001a). Closed-loop control of an HCCI engine. *SAE paper 2001-01-1031*.

Olsson, J.O., Tunestål, P., Haraldsson, G. & Johansson, B. (2001b). A turbo charged dual fuel HCCI engine. *SAE paper 2001-01-1896*.

Rausen, D.J., Stefanopoulou A.G., Kang, J.-M.., Eng, J.A., Kuo, T.W. (2005). A Mean-value model for control of Homogeneous Charge Compression Ignition (HCCI) engines. *ASME Journal of Dynamic Systems, Measurement, and Control*, 127(3), 355-362.

Ravi, N., Roelle, M.J., Liao, H.-H., Jungkunz, A.F., Chang, C.-F., Park, S. & Gerdes, J.C. (2010). Model-based control of HCCI engines using exhaust recompression. *IEEE Transactions on Control Systems Technology*, 18(6), 1289-1302.

Ravi, N., Liao, H.-H., Jungkunz, A.F., Widd, A., Gerdes, J.C. (2012). Model predictive control of HCCI using variable valve actuation and fuel injection. *Journal of Control Engineering Practice*. 20(4), 421-430.

Shahbakhti, M., Lupul, R. & Koch, C. R. (2007a). Sensitivity analysis and modeling of HCCI auto-ignition timing. *Proceeding of the Fifth IFAC Symposium on Advances in Automotive Contro*l, 303–310, August 2007, Monterey coast, California.

Shahbakhti, M. & Koch, C.R. (2007b). Thermo-kinetic combustion modeling of an HCCI engine to analyze ignition timing for control applications. *Proceeding of Combustion Institute/Canadian Section (CI/CS) Spring Technical Conferenc*e, May 2007.

Shahbakhti, M. & Koch, C. R. (2008). Characterizing the cyclic variability of ignition timing in an HCCI engine fueled with n-Heptane/iso-Octane blend fuels. *International Journal of Engine Research*, 9(9), 361–397.

Shahbakhti, M. (2009). *Modeling and experimental study of an HCCI engine for combustion timing control*. Ph.D. Thesis, University of Alberta.

Shahbakhti, M., Ghazimirsaied, A. & Koch, C.R. (2010a). Experimental study of exhaust temperature variation in a Homogeneous Charge Compression Ignition Engine. *Proceeding of the IMechE Part D: Journal of Automobile Engineering*, 224(9), 1177-1197.

Shahbakhti, M. & Koch, C.R. (2010b). Physics based control oriented model for HCCI combustion timing. *ASME Journal of Dynamic Systems, Measurement and Control*, 132 (2), 021010.

Shahbakhti, M., Ghazimirsaied, A. & Koch, C.R. (2011). Modeling ranges of cyclic variability for HCCI ignition timing control. *Proceedings of the ASME 2011 Dynamic Systems and Control Conference*, paper DSCC2011-6118, October 31 - November 2, Arlington, VA.

Shaver, G. M., Gerdes, J.C., Jain, P., Caton, P.A. & Edwards, C.F. (2005a). Dynamic modeling of HCCI engines utilizing variable valve actuation. *ASME Journal of Dynamic Systems, Measurement and Control*, 127(3), 374-381.

Shaver, G. M., Roelle, M., Gerdes, J.C. (2005b). Decoupled Control of Combustion Timing and Work Output in Residual-Affected HCCI Engines. *2005 American Control Conference*, June 8-10. Portland, OR, USA.

Shaver, G. M., Roelle, M. J. & Gerdes, J. C. (2006). Modeling cycle-to-cycle dynamics and mode transition in HCCI engines with variable valve actuation. *Journal of Control Engineering Practice*, 14, 213-222.

Shaver, G.M. (2009a). Stability analysis of residual-affected HCCI using convex optimization. *Journal of Control Engineering Practice*, 17, 1454-1460.

Shaver, G. M., Gerdes, J. C. & Roelle, M. J. (2009b). Physics-based modeling and control of residual-affected HCCI engines. *ASME Journal of Dynamic Systems, Measurement and Control*, 131(2), 021002.

Sira-Ramirez, H. (1991). Nonlinear discrete variable structure systems in quasi sliding mode. *International Journal of Control*, 54(5), 1171–1187.

Stanglmaier, R. H. & Roberts, C. E. (1999). Homogeneous Charge Compression Ignition (HCCI): benefits, compromises and future engine applications. *SAE paper 1999-01-3682*.

Strandh, P., Bengtsson, J., Johansson, R., Tunestål, P. & Johansson, B. (2004). Cycle-to-cycle control of a dual fuel HCCI engine. *SAE paper 2004-01-0941*.

Strandh, P., Bengtsson, J., Johansson, R., Tunestål, P. & Johansson, B. (2005). Variable valve actuation for timing control of a HCCI engine. *SAE paper 2005-01-0147*.

Su, W. C., Drakunov, S. V., and Özgüner, Ü. (2000). An O (T 2) boundary layer in Sliding Mode for sampled-data system. *IEEE Transactions on Automatic Control*, 45 (3), 482-485.

Swan, K., Shahbakhti, M. & Koch, C.R. (2006). Predicting start of combustion using a modified knock integral method for an HCCI engine. *SAE 2006 Transactions Journal of Engines*, 611-620.

Widd, A., Liao, H.-H., Gerdes, J.C., Tunestål, P. & Johansson, R. (2011). Control of exhaust recompression HCCI using hybrid model predictive control. *2011 American Control Conference*, June 29-July 1, San Francisco, CA.

Widd, A., Ekholm, K., Tunestål, P. & Johansson, R. (2012). Physics-based model predictive control of HCCI combustion phasing using fast thermal management and VVA. *IEEE Transactions on Control Systems Technology*, 20 (3), 688-699.

Xingcai, L., Yuchum, H., Libin, J., Linlin, Z. & Zhen, H. (2006). Heat release analysis on combustion and parametric study on emissions of HCCI engines fueled with 2-Propanol/n-heptane blend fuels. *Energy Fuels*, 20(5), 1870–1878.

Yang, X., Zhu, G. G. (2011). A two-zone control oriented SI-HCCI hybrid combustion model for the HIL engine simulation. *2011 American Control Conference*, June 29-July 1, San Francisco, CA.

Yao, M., Zheng, Z., Zhang, B. & Chen, Z. (2004). The effect of PRF fuel octane number on HCCI operation. *SAE paper 2004-01-2992*.

Youcef-Toumi, K., and Ito, O., (1990). A time delay controller for systems with unknown dynamics. *ASME, Journal of Dynamic Systems, Measurement, and Control*, 112, 133-142.

Yu, W.-C. & Wang, G.-J. (2006). Discrete sliding mode controller design based on the LQR suboptimal approach with application on AC servo motor. *Journal of the Chinese Institute of Engineers*, 29(5), 873-882.

Zhao, F., Asmus, T. W., Assanis, D. N., Dec, J. E., Eng, J. A. & Najt, P. M. (2003). Homogeneous charge compression ignition (HCCI) engines. *SAE publication PT-94*.

Zhao, H. (2007). *HCCI and CAI engines for the automotive industry*. Florida: CRC Press.

Acronyms

aBDC	after Bottom Dead Center
aTDC	after Top Dead Center
BDC	Bottom Dead Center
CAD	Crank Angle Degrees
$\boldsymbol{CA50}$	Crank Angle for 50% burnt fuel
CO	Carbon Monoxide
DSSMC	Discrete Sub-optimal Sliding Mode Controller
EGR	Exhaust Gas Recirculation
EOC	End of Combustion
EVC	Exhaust Valve Closing
EVO	Exhaust Valve Opening
HCCI	Homogenous Charge Compression Ignition
IVC	Intake Valve Closing
IVO	Intake Valve Opening
LQG	Linear Quadratic Gaussian
LQR	Linear Quadratic Regulator
MKIM	Modified Knock Integral Model
MPC	Model Predictive Controller
NO_x	Nitric Oxides
ON	Octane Number
PI	Proportional Integral
PID	Proportional Integral Derivative
PM	Particulate Matter
PRF	Primary Reference Fuel
SMC	Sliding Mode Controller
SOC	Start of Combustion
TDC	Top Dead Center
UHC	Unburned Hydrocarbon

Symbols

AFR	air-fuel ratio [-]
$\bar{C}_v$	average constant-volume specific heat capacity [kJ/kg K]
$CA50$	crank angle for 50% burnt fuel [CAD aTDC]
CoC	completeness of combustion [%]
ΔT_{comb}	temperature increase due to the combustion process [K]

EGR	Exhaust gas recirculation fraction
K_I	integral control gain in PI control
K_p	proportional control gain in PI control
l	gain vector of Kalman filter
LHV	low heating value [kJ/kg]
m	[kg] but [g] in Table 3 and Fig. 9
n	ratio of specific heat capacities [-]
N	engine speed [rpm]
N_u	feed-forward gain vector
ON	fuel octane number [-]
P	pressure [kPa]
$\emptyset$	fuel equivalence ratio [-]
$\bar{R}$	average gas constant [kJ/kg K]
X_r	residual gas fraction [-]
ρ	density [kg/m^3]
T	temperature [K] but [°C] in Eq. (5) and (6)
θ	crank angle [CAD]
x	model state vector
V	volume [m^3]
w	physical disturbance vector

Subscripts

comp	compression
comb	combustion
e	expansion
eoc	end of combustion
evc	exhaust valve closing
evo	exhaust valve opening
f	fuel
iso	iso-Octane
ivc	intake valve closing
ivo	Intake valve opening
k	engine cycle index
m	manifold
mix	mixture
nc	new charge to the engine cylinder
nH	n-Heptane
rg	Residual gas
r	reference
soc	start of combustion
st	stoichiometric
t	total mixture

Appendix A: Model Parameters

PRFs' Properties and Average Specific Heat Capacities and Gas Constants

Table A.1 Fuel and in-cylinder gas properties

Subscript	$\overline{C}_v$ [kJ/kgK]	R [kJ/kgK]	LHV [kJ/kg]	ρ [kg/m^3]
iso	-	-	4.434 e+4	6.900 e+2
nH	-	-	4.456 e+4	6.820 e+2
nc	7.700 e-1	-	-	-
rg	8.180 e-1	-	-	-
ivc	-	2.860 e-1	-	-
soc	-	2.890 e-1	-	-
eoc	-	2.870 e-1	-	-
evc	-	2.893 e-1	-	-

Constants of P_{ivc} and T_{ivc} Correlations (Eq. (1) and Eq. (2))

a= 0.027 b= 0.046 c= 0.005

Table A.2 Values of constants for T_{ivc} correlation

constant	PRF0	PRF10	PRF20	PRF40
a_1	-7.300 e-3	-1.700 e-3	-1.700 e-3	-7.000 e-4
a_2	1.482	4.073 e-1	5.533 e-1	3.470 e-1
a_3	1.103 e+2	1.012 e+2	1.134 e+2	1.123 e+2
b_1	-1.488 e-1	-4.310 e-2	-1.164 e-1	-5.100 e-3
b_2	-8.500 e-2	-1.620 e-2	-4.260 e-2	-1.750 e-2
b_3	9.200 e-3	2.400 e-3	2.000 e-4	1.200 e-3

$CA50$ Correlation

Constant coefficients of Eq. (11) are C_1= -0.67, C_2= 219.0, C_3= 0.328, C_4= 28.4. Here is a discussion on these constant coefficients:

There is a direct relation between ON and the auto ignition phasing as an increase in ON leads to delay in combustion phasing (Shahbakhti et al., 2008; Chiang et. al, 2007). The positivity of C_3 conveys such a trend. On the other hand, based on the experimental results on the same studied engine in (Audet et al., 2009), there is an approximate linear relation between variations of $CA50$ and the inducted fuel mixture ON. The results in (Audet et al., 2009) show that the sensitivity of this linear relation is approximately constant at different operating conditions which justfies the constant value of C_3.

HCCI combustion has a compression ignitition nature and an increase in T_{mix} leads to earlier combustion phasing and vice versa. Negative value of C_2 implies such a negative relation between variations of $CA50$ and T_{mix}. Simulation results of MKIM from the physical model show an approximate linear relation between $CA50$ and T_{mix} (Fig.A.1). Such an approximate linear relation is also been seen in other studies (Chiang et al., 2007; Ravi et al., 2010).

Any increase in the amount of inducted fuel energy which can be implicated by $\emptyset$ leads to an advance in combustion phasing (Chiang et. al, 2007; Shahbakhti et al., 2008). Value of $(C_1\ T_{mix} + C_2)$ as the coefficient of $\emptyset$ is negative in the normal operatting range of this engine, which justfies such a negative relation.

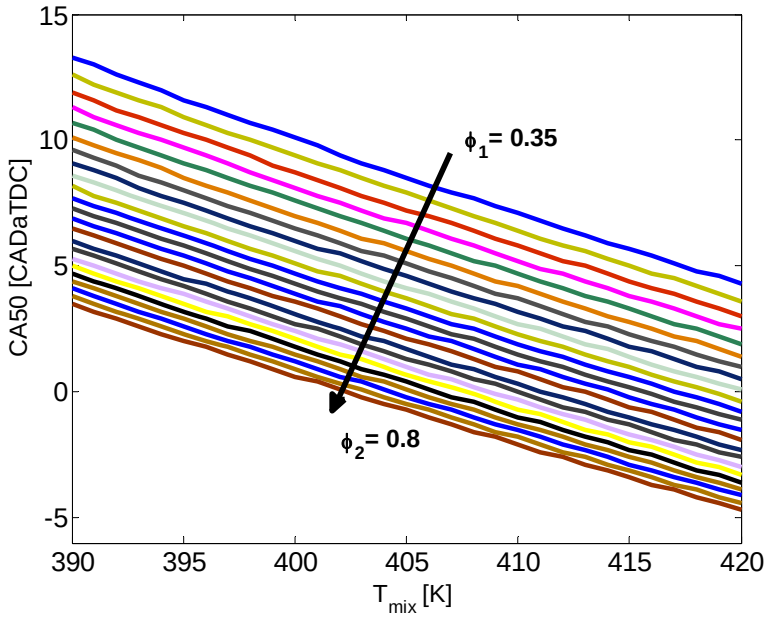

Fig. A.1. MKIM simulation (ON= 5, N= 800 rpm)

Appendix B: Selection of PI Controller Gains

Variations in the controller gains are shown in Figures B.1 and B.2. These two figures show that for the selected values of gains ($\mathrm{K_i} = 5.35, \mathrm{K_p} = 0.08$), optimum control metrics including the maximum overshoot and rise time are achievable around the studied nominal operating point.

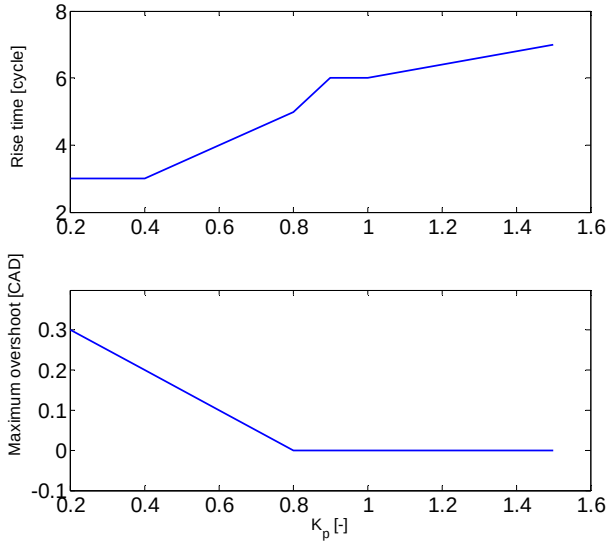

Fig. B.1. Variation of control metrics for different values of K_p ($K_i = 5.35$)

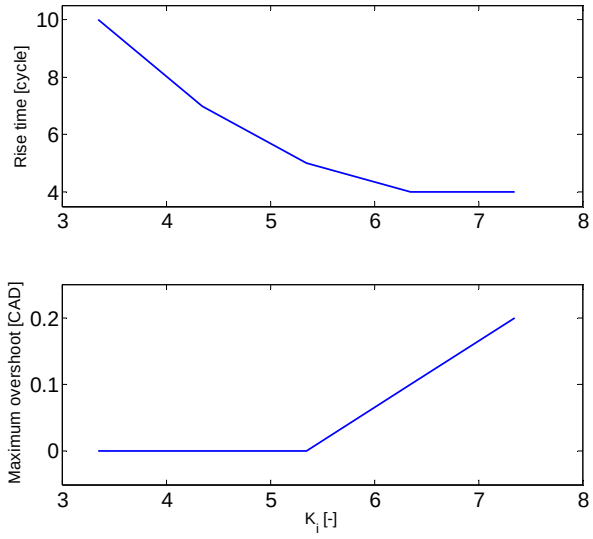

Fig. B.2. Variation of control metrics for different values of K_i ($K_p = 0.08$)